*Exploration Geophysics (2006) **37**, 10-18*
Butsuri-Tansa (Vol. 59, No. 1)
Mulli-Tamsa (Vol. 9, No. 1)

Laboratory study of CO_2 migration in water-saturated anisotropic sandstone, based on P-wave velocity imaging

Ziqiu Xue [1], Xinglin Lei [2]

Key Words: Difference tomography, P-wave velocity, porous sandstone, CO_2 monitoring, bedding plane, anisotropy

ABSTRACT

We measured the changes in P-wave velocity that occur when injecting CO_2 in gaseous, liquid, and supercritical phases into water-saturated anisotropic sandstones. P-wave velocities were measured in two cylindrical samples of Tako Sandstone, drilled along directions normal and parallel to the bedding plane, using a piezo-electric transducer array system. The velocity changes caused by CO_2 injection are typically -6% on average, with maximum values about -16% for the case of supercritical CO_2 injection. P-wave velocity tomograms obtained by the differential arrival-time method clearly show that CO_2 migration behaviour is more complex when CO_2 flows normal to the bedding plane than when it flows parallel to bedding. We also found that the differences in P-wave velocity images were associated both with the CO_2 phases and with heterogeneity of pore distribution in the rocks. Seismic images showed that the highest velocity reduction occurred for supercritical CO_2 injection, compared with gaseous or liquid CO_2 injection. This result may justify the use of the seismic method for CO_2 monitoring in geological sequestration.

INTRODUCTION

Sequestration of Carbon Dioxide (CO_2) into saline aquifers has been proposed as one of the most practical options of all geological sequestration possibilities. When saline aquifers are to be used to sequester CO_2 for long periods, it will be necessary to monitor the migration and diffusion of CO_2 in those reservoirs. Monitoring of geological sequestration has been identified as one of the highest priority needs in several recent international conferences on greenhouse gas control technologies. Monitoring is necessary to confirm the containment of CO_2, to assess leakage paths, and to gain understanding of interactions between CO_2, the rock-forming minerals, and formation fluids (Benson, 2005). Monitoring is also necessary to quantify the net quantity of CO_2 that has been sequestered within the reservoirs (Chadwick et al., 2004). Seismic surveys provide the most attractive approach for obtaining the spatial coverage required for mapping the location and movement of CO_2 in the subsurface (Arts et al., 2004; Li, 2003; Saito et al., 2005). However, the effectiveness of these techniques depends upon many factors, including the contrast between the physical properties of CO_2 and resident formation fluids, the lithology and structure of the reservoir, formation fluid pressure and temperature variations, source and receiver locations, well spacing, and injection patterns (Hoversten and Myer, 2000).

When CO_2 is injected into an aquifer, the existing formation water in pore spaces of the reservoir rock will be partially displaced by the CO_2. This process will result in local reduction of the velocity of seismic waves propagating through the reservoir (Wang et al., 1998; Arts et al., 2004). Crosswell seismic surveying has been one of the earliest applications of time-lapse geophysics to map the movements of injected CO_2 in enhanced-oil-recovery processes (e.g., Harris et al., 1995). Because seismic data with frequencies up to a few kilohertz can potentially offer imaging resolution of the order of metres, such as is often necessary for time-lapse investigation, seismic methods are useful in building reservoir models and for accurately describing fluid flow in heterogeneous reservoirs. For these reasons, a time-lapse crosswell seismic survey has been conducted to monitor CO_2 at a pilot-scale injection site in Nagaoka, Japan (Saito et al., 2005).

The process of injection of CO_2 into saline aquifers can be described as immiscible displacement of an aqueous phase by a less dense and less viscous gas phase. The density and viscosity of the CO_2 are the two key factors dominating the displacement process (Van der Meer, 1992). Both of them are functions of temperature and pressure in reservoirs. The phase diagram of CO_2 shows a critical temperature of 31°C and a critical pressure of 7.38 MPa. Under usual geological conditions, the temperature and pressure in a reservoir deeper than 800 m are expected to be above the critical values, and CO_2 will be in a supercritical state. Supercritical CO_2 is characterised by a gas type of kinetic behaviour with a liquid type of density. The general view is that whatever the reservoir conditions is, the ratios of both density and viscosity between formation water and CO_2 are larger than unity. Therefore, on the large scale, the density difference will result in gravity segregation, and the viscosity difference will result in hydrodynamically unstable displacement between formation water and the CO_2 (Garcia and Pruess, 2003).

This paper reports an experimental study of seismic monitoring of CO_2 in water-saturated porous sandstones (Xue and Ohsumi, 2004a, 2005). Measurements of P-wave velocity were made on two samples of Tako Sandstone, one sample cut with the axis normal and one with the axis parallel to the bedding plane. The goal of this paper is to improve understanding of the P-wave velocity decrease caused by CO_2 injection, by comparing the differences in seismic images reconstructed from P-wave velocity changes during injection of gaseous CO_2, liquid CO_2, and supercritical CO_2 into the same sample. Tako Sandstone, used in this study, is less affected by changes of confining pressure and pore pressure, and thus the displacement process would be expected to take place within almost the same pore spaces of each sample (Xue and Ohsumi, 2004b). Change of seismic velocity reflects the difference in bulk moduli between CO_2 and water, and the fraction of CO_2 present. In this study, the P-wave velocity changes in partially saturated conditions for each sample were reconstructed precisely using differential arrival-time tomography.

[1] *Research Institute of Innovative Technology for the Earth (RITE)*
9-2 Kizugawadai, Kizu-cho, Soraku-gun,
Kyoto, 619-0292 JAPAN
Phone: +81-774-75-2312
Facsimile: +81-774-75-2313
Email: xue@rite.or.jp

[2] *Geological Survey of Japan, National Institute of Advanced Industrial Science and Technology (AIST)*
Central 7, Higashi 1-1, Tsukuba City,
Ibaraki, 305-8567 Japan

Manuscript received 21 September, 2005.
Revised manuscript received 15 December, 2005.
Part of this paper was presented at the 108th SEGJ Conference (2003).

SAMPLES AND EXPERIMENTAL PROCEDURE

Two cylindrical samples of Tako Sandstone (50 mm in diameter and 105 mm in length, 24% porosity) were used in this study. In order to examine roles of the bedding plane in CO_2 injection, the samples, referred to as TS-4 and TS-5, were drilled normal and parallel to the bedding plane, respectively. Sixteen piezo-electric transducers (PZTs) with a characteristic frequency of 1 MHz were cemented onto the surface of each sample, in two parallel lines along the axial direction (Figure 1a). In sample TS-5 the PZT array was located along the bedding plane. Figure 1b shows the diagram of ray paths for P-wave velocity measurement, and cell geometry for P-wave velocity tomography. Two-dimensional models of relative P-wave velocity change during CO_2 injection into the water-saturated rock were reconstructed using the difference tomography method. P-wave velocities were measured at a time interval of 3 to 5 minutes during CO_2 injections into the water-saturated samples.

Stainless-steel end pieces were attached to both sample ends, and a grooved plate was placed between the end piece and the sample at each end. Concentric grooves connected by radial grooves were carved on the plate surface to ensure uniform injection over the entire surface of the sample end. The sample assembly was sealed with silicone sealant to prevent infiltration of oil, which was used as the hydrostatic pressure medium. Initially, each sample was saturated by injection of fresh distilled water from the top end. Then, CO_2 was introduced at the bottom end of each sample, at different pressure and temperature conditions corresponding to gas, liquid, and supercritical phases. These conditions are referred to as cases I, II, and III, respectively (Table 1). Before the case II and III experiments, the sample was flooded with fresh distilled water to remove the residual CO_2 from the previous CO_2 injection. See Xue and Ohsumi (2004a) for more details of the measurement system and experimental procedure, including CO_2 injection and pressure variation.

DATA PROCESSING

Picking of P-wave arrival times

The accuracy of relative arrival times is very important in this study, because our major purpose is to investigate the changes in the P-wave velocity field resulted from the fluid displacement processes. To determine P-wave travel times precisely, a graphical user interface (GUI) software tool *TSpro* (Lei, <http://staff.aist.go.jp/xinglin-lei/Lei00.htm>) was used in this study. Initially, the P-wave arrival times of the first measurement during each injection run were automatically determined, using an algorithm based on an AR time-series model. Then every arrival time was checked and corrected manually. For the second and later measurements, the arrival time for each path was determined manually by interactive waveform comparison using the GUI tool. The two waveforms for two consecutive measurements on each path were displayed together, and the arrival time of the later measurement was determined by comparing the waveform of the first one or two oscillations after the first P-wave arrival. This process was repeated several times on the two waveforms to ensure the arrival time was determined properly. This procedure improved greatly

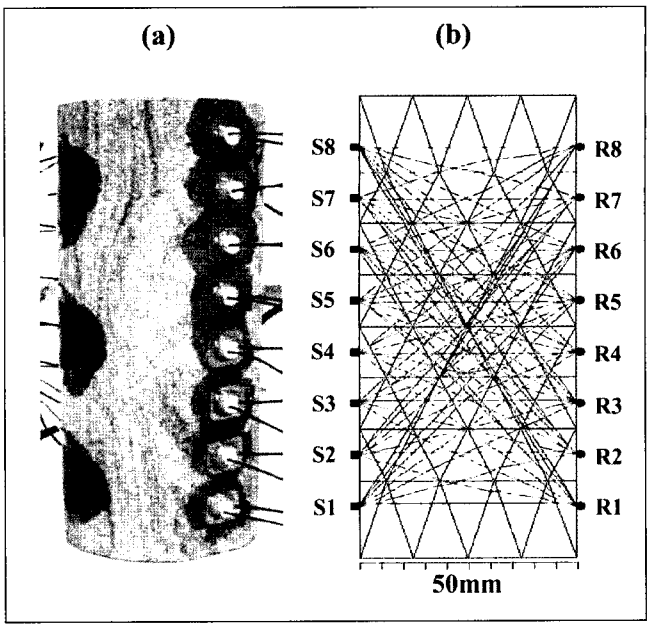

Fig. 1. a) Strain gauges and PZT transducers mounted on a test sample. b) A schematic diagram of two-dimensional P-wave tomography. Ray paths (blue) for P-wave velocity measurements and cell geometry (black) for tomography are shown. The source and receiver positions are indicated by S1-S8 and R1-R8, respectively.

the relative accuracy of P-wave arrival times, especially for longer ray paths. Figure 2 shows an example of typical waveforms and their arrival times determined by these procedures, for several paths during injection of gaseous CO_2 into the water-saturated sample TS-4. In Figure 2, along path S1-R4, the signal-to-noise ratio is very low around the first motion of P-wave. In such a case, waveform comparison is very efficient.

Velocity Tomography

In order to improve the accuracy of measurement of relative changes of P-wave velocity caused by CO_2 injection, the following difference tomography method was applied in this study. The body-wave travel time T_{ij} along the ray path from the i-th source to the j-th receiver is expressed as a path integral

$$T_{ij} = \int_l p \, ds \quad , \tag{1}$$

where p is the slowness (the inverse of velocity), l_{ij} is the ray path between the source and receiver corresponding to the assumed P-wave velocity model, and ds is an element of distance along the path. The travel time difference ΔT_{ij} due to P-wave velocity change Δp is given by

$$\Delta T_{ij} = T_{ij} - T'_{ij} = \int_l p \, ds - \int_l (p + \Delta p) \, ds \quad . \tag{2}$$

For small Δp and as a first order approximation, the change of ray path caused by velocity change is ignored, so that ΔT_{ij} is expressed approximately by

$$\Delta T_{ij} \approx \int_l \Delta p \, ds \quad . \tag{3}$$

Case	Hydrostatic pressure (MPa)	Pore pressure (MPa)	CO_2 injection pressure (MPa)	Temperature of injected CO_2 (°C)
I	10	3	5	23
II	10	6	8	23
III	15	10	12	34

Table 1. Pressure and temperature conditions for the three CO_2 injection experiments.

Using equation (3) Δp can be determined directly from ΔT with a simultaneous iterative reconstruction technique (SIRT), similar to the classic travel-time tomography method based on equation (1). It is clear that the effects of error in the slowness p are partly cancelled.

It is important to use an optimum initial model in order to obtain a plausible reconstructed model. The initial model for each case of CO_2 injection was constructed using the travel times obtained from the water-saturated samples before CO_2 injection, using the SIRT method based on equation (1). Since both samples TS-4 and TS-5 have a strong anisotropy of P-wave velocity resulted from the bedding structure, the SIRT method was modified to take anisotropy into consideration. In anisotropic (transversely isotropic) rocks, P-wave velocity depends only on the angle from the symmetry axis. We used a simple assumption described by

$$V(\theta) = V_{\min}\left(1 + \varepsilon \sin^2\theta\right) , \quad (4)$$

$$\varepsilon = \left(V_{\max} - V_{\min}\right)/V_{\min} , \quad (5)$$

where θ is the angle between the ray path and the normal to the bedding plane, ε expresses the degree of anisotropy, and $V_{\max}$ and $V_{\min}$ correspond to the P-wave velocities along the bedding plane and along the direction normal to the bedding plane, respectively. As mentioned above, sample TS-4 was drilled with its axis normal to the bedding plane, while sample TS-5 was drilled with its axis parallel to the bedding plane. It is important for further discussion to note that $V_{\max}$ in TS-4 is in the diameter direction, while $V_{\max}$ in TS-5 is in the axial direction. For a given ε, V_{max} is a linear function of V_{min}:

$$V_{\max} = (1+\varepsilon)V_{\min} . \quad (6)$$

As mentioned in the introduction, the physical properties of Tako Sandstone are less affected by changes of confining pressure and pore pressure, and thus the pore structures would not change during the experiment (Xue and Ohsumi, 2004b). Consequently, it is reasonable to assume that the direction of V_{max} or V_{min} did not change with time during the CO_2 injection. In general, it is necessary to determine both V_{max} and V_{min}. However, in such cases, the number of unknown parameters would be twice as many as in the isotropic case. In the P-wave velocity measurement here, there are only 64 ray paths and no vertical paths. In order to reconstruct a reliable velocity field with such limited observation data, the inversion problem is simplified by assuming that the degree of anisotropy (ε) does not change during fluid injection. This issue will be discussed further in the sections following. For constant ε, velocity changes in V_{max} and V_{min} are related by

$$dV_{\max} = (1+\varepsilon)\, dV_{\min} \quad (7)$$

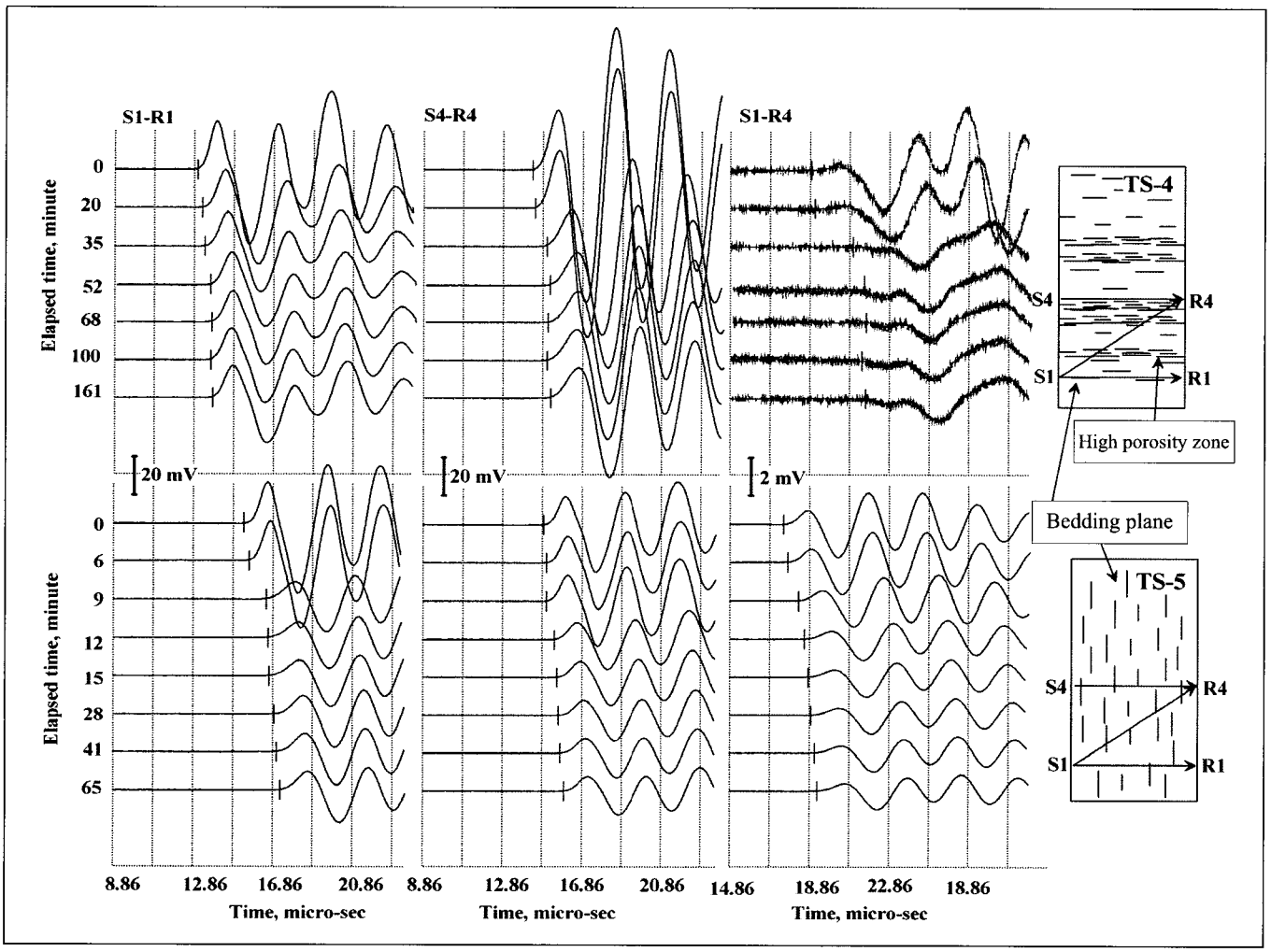

Fig. 2. Examples of waveforms measured along three paths S1-R1, S4-R4, and S1-R4 in the samples TS-4 and TS-5 during injection of gaseous CO_2. The short vertical bar in each waveform indicates the first arrival time, which was determined manually by interactive waveform comparison of two consecutive measurements. A schematic diagram that shows the basic features of the samples is also plotted beside the waveforms. In sample TS-4, there are several horizontal zones of greater porosity, which enhanced the bulk anisotropy of the seismic velocity.

Equation (7) contradicts theoretical and experimental results where most velocity changes in anisotropic media show large velocity changes in the V_{min} direction. However, in our experiments, we treat only change in relative velocity, and the assumption of equation (7) does not affect the major results. In order to determine the optimum value of ε for each injection experiment, the SIRT method was applied to the travel-time data for: 1) dry sample, 2) water-saturated sample, and 3) the final stage of each CO_2 injection experiment. Values of ε from 0 (isotropic model) to 0.3 were examined for each data set. Figure 3 shows the mean square error of the residual times of the reconstructed velocity models, as a function of ε, for sample TS-5. The optimum value of ε was that associated with the minimum mean square error. For the dry (Dry) and water-saturated (W) conditions, the estimated ε were 0.15 and 0.075, respectively. After the gaseous CO_2 injection (G), the optimum value of ε was estimated to be 0.1. Since our major interest is the velocity change when injecting CO_2, into the water-saturated sample, the value $\varepsilon = 0.075$ obtained from the water-saturated sample was used in difference tomography for sample TS-5. For sample TS-4, ε was determined to be 0.2 in the same manner. It is noticeably larger than ε for TS-5, although both TS-4 and TS-5 were drilled from the same Tako Sandstone. In fact, there are several horizontal zones with comparative high porosity in sample TS-4 (Figure 2). Such microscopic heterogeneity greatly enhanced the bulk anisotropy of the sample. Therefore, the reconstructed velocity model in Figure 4, using the optimum ε of 0.2 is better than the isotropic model, and it also shows fewer false images than other values.

EXPERIMENTAL RESULTS

P-wave velocity reduction caused by CO_2 injection

The CO_2 was injected into the water-saturated samples at different pressure and temperature conditions referred to as cases I, II and III in Table 1. The P-wave velocity decreased clearly during CO_2 injection in all cases. For TS-4, where all paths are parallel to the bedding plane of the sample, the results correspond to the decrease of V_{max}. On the other hand, for TS-5, the results correspond to the decrease of V_{min}. Figure 5 shows the P-wave velocity reduction obtained along the eight shortest paths (S1-R1, S2-R2, S3-R3, S4-R4, S5-R5, S6-R6, S7-R7, and S8-R8) during

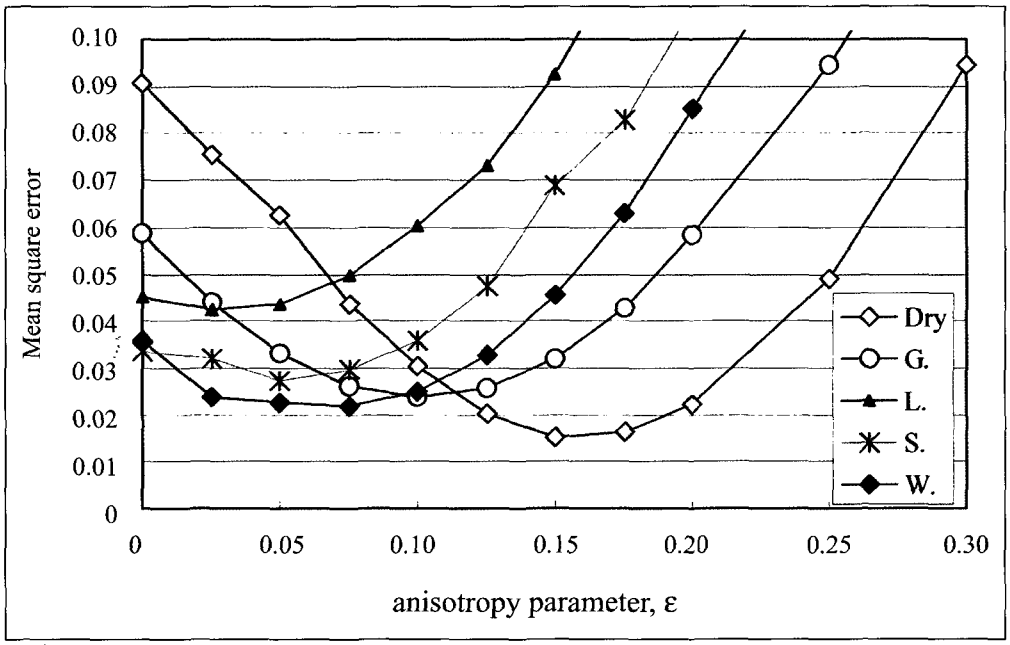

Fig. 3. Example of variation of the mean square error in travel-time residuals in tomography, with respect to the anisotropy parameter ε. The value of ε associated with the minimum mean square error was used as a measure of the anisotropy parameter in each case. "Dry" and "W" refer to the dry and water-saturated conditions, respectively. G, L, and S refer to gaseous, liquid and supercritical CO_2 injection experiments, respectively.

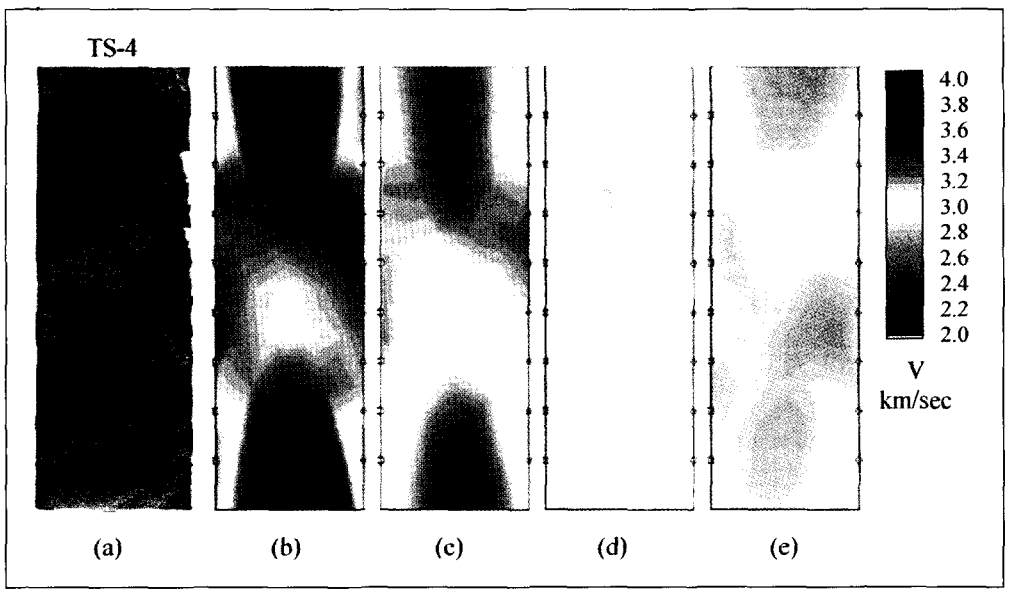

Fig. 4. A photo image of the cut surface along the PZT array of the TS-4 sample (a) and the reconstructed velocity (V_{min}) model, using data measured on the water-saturated TS-4 sample. Panels b–e indicate results using different values of ε (b: 0.0, c: 0.1, d: 0.2, e: 0.3). Note that $\varepsilon = 0.2$ resulted in the minimum residual and the most reliable model, coinciding with the macroscopic structures in the sample.

injection of supercritical CO_2 into both samples. Those P-wave velocities were measured directly from waveforms by picking the arrival times. Figure 5 shows that, when the front of migrating CO_2 reached a ray path, a significant decrease appeared in the P-wave velocity along that path. The difference in time lags between the commencement of velocity reduction in the two samples indicates that the CO_2 front moved faster in TS-5 than in TS-4. The P-wave velocity reductions are summarised in Tables 2 and 3. In sample TS-4 the final P-wave velocity decrease ranged from 4.3 to 6.5% for the gaseous CO_2 injection, 4.9 to 9.5% for the liquid CO_2 injection and 6.1 to 10.6% for the supercritical CO_2 injection, except for the path S7-R7 where only small velocity reductions were observed. P-wave velocities decreased much more in TS-5 than in TS-4 for all cases, although both samples were subjected to the same pressure and temperature conditions. The larger velocity reduction in TS-5 results from anisotropy in the Tako Sandstone, because P-wave velocity reduction is larger in the direction normal to the bedding plane. Most narrow pores are aligned with their planes parallel to the bedding plane (Hudson, 1981; Nishizawa, 1982).

P-wave velocity imaging of CO_2 migration in the water-saturated sample

Figures 6–8 show the distribution of velocity change at selected time intervals during gaseous, liquid, and supercritical CO_2 injections in TS-4 (upper) and TS-5 (lower), respectively. In all cases, the upward CO_2 migration in each sample was clearly imaged. All injection experiments in each sample show similar distributions of velocity change along the profile. The common outcomes are summarised as follows:

1) Most parts of the profiles showed negative velocity changes, ranging from 0 to -0.4 km/s.
2) Especially in TS-5, there was a comparatively larger velocity decrease around the ends of the sample.
3) After breakthrough of CO_2 at the top end, P-wave velocity continued to decrease slowly and finally reached a stable level after 30 and 100 minutes for TS-5 and TS-4, respectively.
4) Movement of CO_2 in TS-5 was about twice as fast as in TS-4.

During the injection of gaseous CO_2 into sample TS-5, a velocity decrease appeared around the bottom end 15 minutes after starting injection (Figure 6b). The area of negative velocity change expanded with increasing elapsed time, and reached the top end after 27 minutes. This point agrees well with observation by a monitoring video camera of the first CO_2 bubble at the outlet tube. Similar behaviour of P-wave velocity changes was observed for the

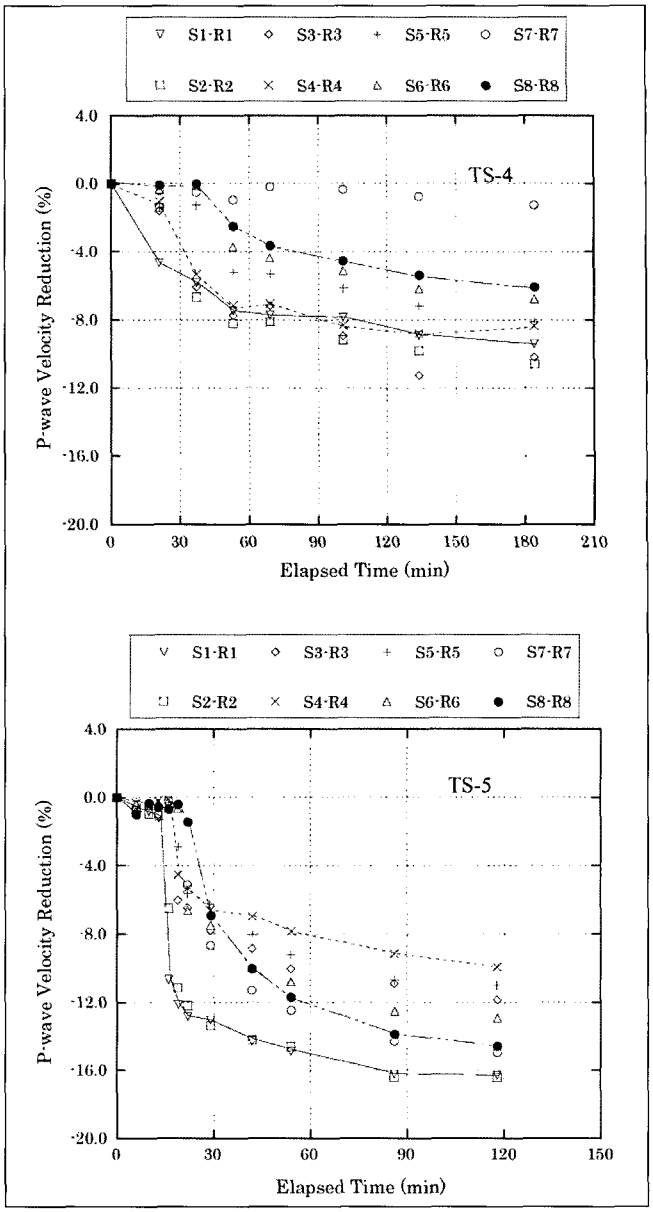

Fig. 5. Lateral P-wave velocity changes with respected to elapsed time during injection of supercritical CO_2 in samples TS-4 (a) and TS-5 (b). Note that the velocity changes correspond to V_{max} in TS-4 but V_{min} in TS-5.

Case	S1-R1	S2-R2	S3-R3	S4-R4	S5-R5	S6-R6	S7-R7	S8-R8
I	-5.8	-6.5	-6.4	-5.6	-4.8	-4.4	-0.8	-4.3
II	-7.6	-9.5	-8.2	-7.5	-5.6	-5.8	-0.5	-4.7
III	-9.4	-10.6	-10.2	-8.4	-8.1	-6.8	-1-3	-6.1

Table 2. Percentage of P-wave velocity reduction during injection of gaseous CO_2, liquid CO_2, and supercritical CO_2 into the water-saturated sample TS-4 (from Xue and Ohsumi, 2004a).

Case	S1-R1	S2-R2	S3-R3	S4-R4	S5-R5	S6-R6	S7-R7	S8-R8
I	-10.7	-11.3	-7.6	-5.8	-7.2	-8.1	-10.0	-9.6
II	-11.1	-15.6	-10.7	-8.1	-9.6	-10.2	-12.0	-11.9
III	-16.4	-16.2	-11.8	-9.9	-10.9	-13.1	-14.8	-14.3

Table 3. Percentage of P-wave velocity reduction during injection of gaseous CO_2, liquid CO_2, and supercritical CO_2 into the water-saturated sample TS-5 (from Xue and Ohsumi, 2005).

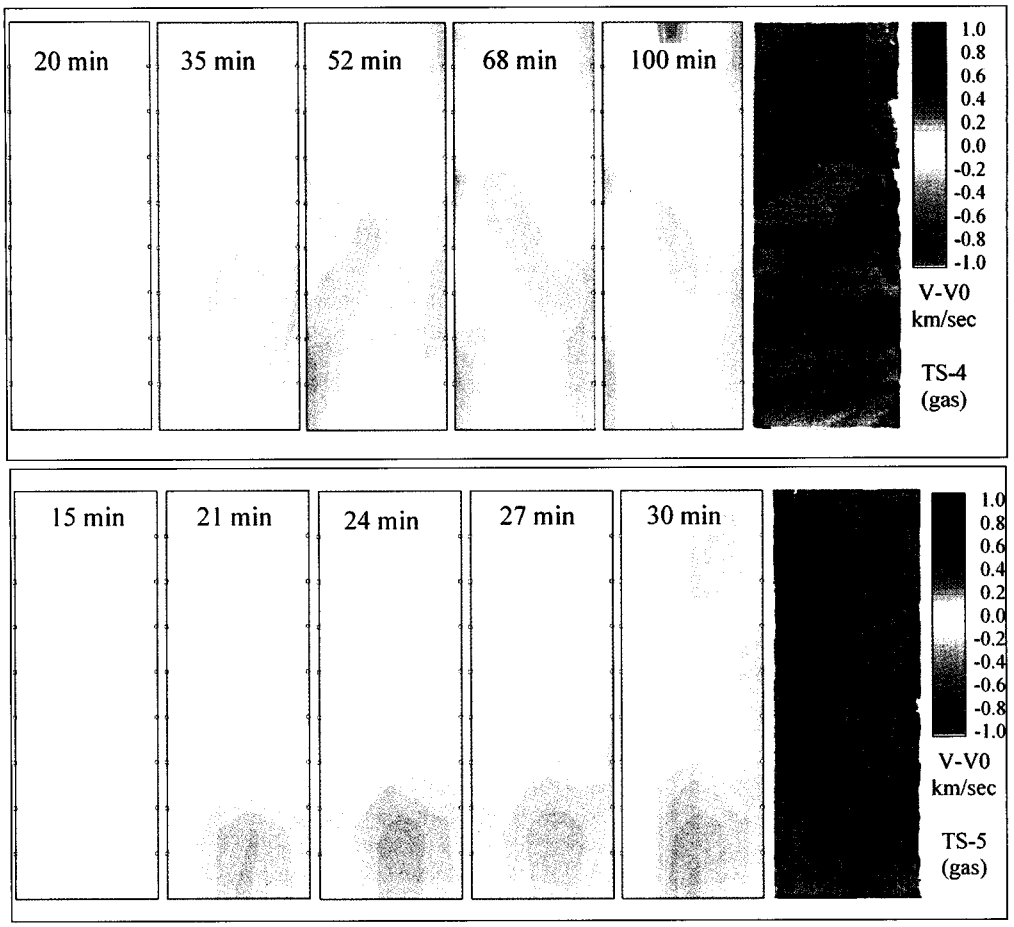

Fig. 6. Reconstructed distributions of velocity change during injection of gaseous CO_2 in the sample TS-4 (upper) and the sample TS-5 (lower). In the left photo, pore space is filled with dyed epoxy, shown by blue colour. In TS-4, areas of larger velocity reduction correspond to areas of higher porosity. In TS-5, distributions of the P-wave velocity changes show good coincidence with the pre-existing macroscopic structure as shown in the right photo.

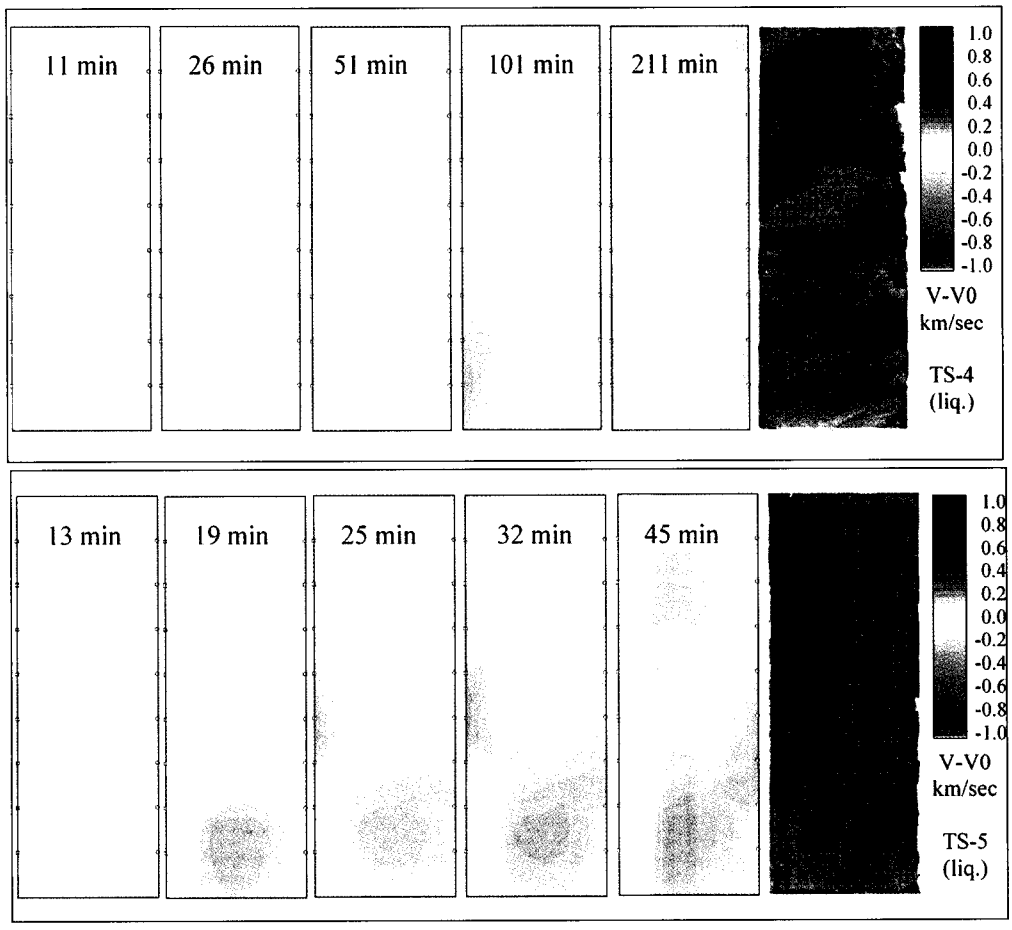

Fig. 7. Reconstructed velocity images during injection of liquid CO_2 in the sample TS-4 (upper) and the sample TS-5 (lower). In the left photo, pore space is filled with dyed epoxy, shown by blue colour. In TS-4, areas of greater velocity reduction correspond to areas of higher porosity. In TS-5 distributions of the P-wave velocity changes show good coincidence with the pre-existing macroscopic structure as shown in the right photo.

injections of liquid and supercritical CO_2 in this sample (Figures 7b, 8b). However, compared with the injection of gaseous CO_2, the final velocity reductions were about twice as large. In TS-4, similar distributions of P-wave velocity change were obtained for all three cases (Figures 6a, 7a, 8a). In TS-5, areas of larger velocity reduction correspond to areas of higher porosity (Figures 6b, 7b, 8b). Velocity reduction in the lower middle and upper left parts was higher than in other part of the profile. There is a preferential flow path at the left side in the middle part of the sample. Such results indicate that the heterogeneity of pore distribution plays an important role on governing CO_2 migration.

DISCUSSIONS AND CONCLUSIONS

P-wave velocity reduction of partially saturated rocks

In partially saturated rocks, seismic wave velocity depends not only on the degree of saturation of CO_2 or water, but also on the microscopic characteristics of saturation. Uniform saturation and patchy saturation have been considered as two extremes (Mavko and Mukerji, 1998). In the strict sense, uniform saturation corresponds to the case that all pores have the same fraction of CO_2 in partially saturated conditions. In contrast, patchy saturation describes the case where some pores are saturated by CO_2 while other pores contain water only. The seismic velocity for such extreme cases can be modelled with Gassmann's Equation (1951). Figure 9 shows the theoretical estimation of P-wave velocity changes as a function of (average) CO_2 saturation, for the Tako Sandstone used in this study. Parameters used in the calculation are from Xue and Ohsumi (2004a). In general, the patchy saturation model and the uniform model correspond to the upper and lower limits of velocity, respectively. In the uniform saturation model, P-wave velocities drastically decrease with the introduction of a small CO_2 fraction, but when the CO_2 fraction is larger than 20% velocities show less change. In the patchy saturation model, P-wave velocities decrease almost linearly with increasing CO_2 fraction.

In addition, the seismic response to partial saturation is also frequency-dependent. If the wavelength of the seismic wave is much longer than the typical patch size, the solid-fluid system can be treated as uniformly saturated. The critical length of patchy saturation is $\sqrt{\kappa K_w / f\mu}$ (Mavko and Mukerji, 1998). In the expression, f is the seismic frequency and κ is the permeability; μ and K_w are the dynamic viscosity and bulk modulus of water, respectively. In this study, the dominant frequency of the elastic waves is about 300 kHz, corresponding to a dominant wavelength of ~10 mm. The critical size is therefore about 3 mm for $\kappa = 10^{-13}$ m^2, $K_w = 2.9\times10^9$ m^{-1}.kg.s^{-2}, $\mu = 8.87\times10^{-4}$ kg.m^{-1}.s^{-1}, and $f = 300\,000$ s^{-1}. Hence, the wavelength is slightly larger than the critical length for patchy saturation, indicating that saturation in these experiments should not be modelled as patchy saturation. Furthermore, the measured P-wave velocity and the tomographic results show that P-wave velocity is very sensitive to the proportion of CO_2 to water in partially saturated conditions. Our experimental results showed an intermediate condition between uniform saturation and patchy saturation in which, for the same CO_2 fraction, liquid and supercritical CO_2 cause larger velocity reduction than gaseous CO_2. Variations of P-wave velocity reduction along the eight shortest paths (Tables 2 and 3) and the reconstructed velocity models (Figures 6–8) also demonstrated a spatially heterogeneous distribution of P-wave velocity in the partially saturation condition. By comparing the pore space distribution in sample TS-5, we found that a larger velocity reduction appeared in a higher porosity area.

In sample TS-4, it is worthwhile to note that P-wave velocity along the path S7-R7 showed significantly smaller change than

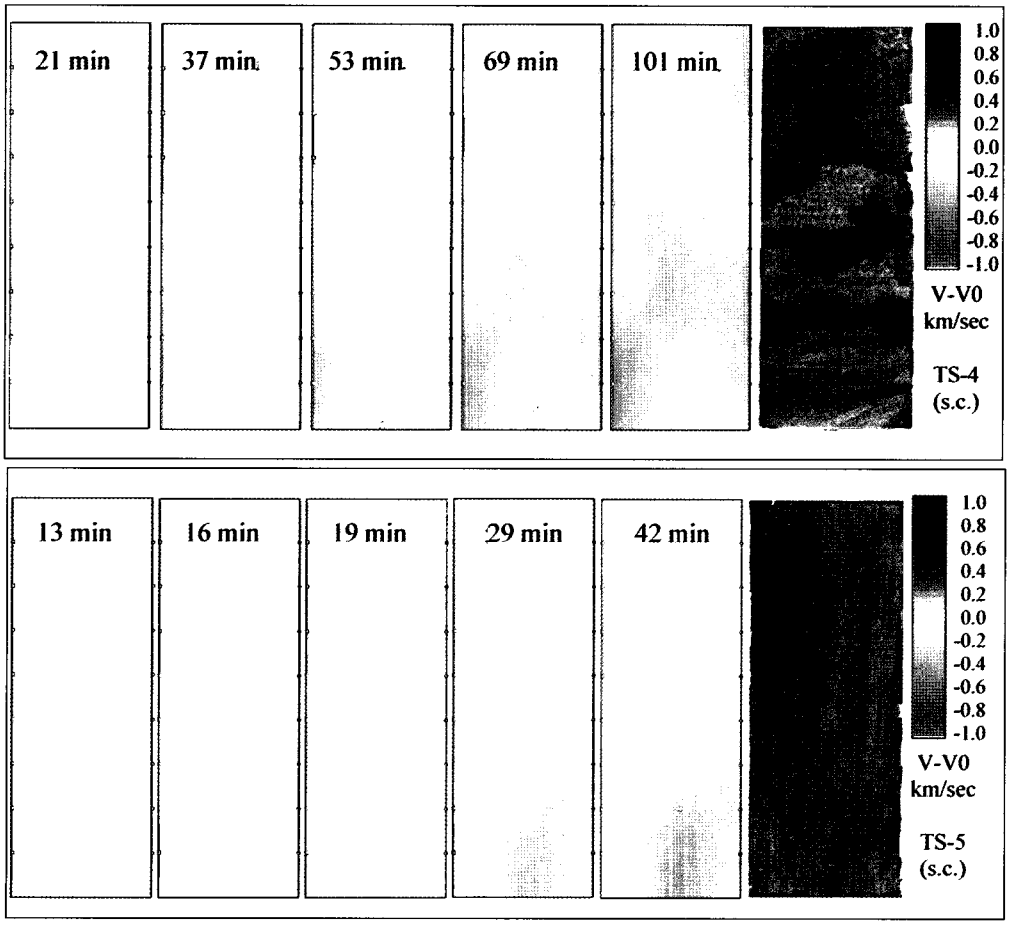

Fig. 8. Reconstructed velocity images during injection of supercritical CO_2 in the sample TS-4 (upper) and the sample TS-5 (lower). In the left photo, pore space is filled with dyed epoxy, shown by blue colour. In TS-4, areas of greater velocity reduction correspond to areas of higher porosity. In TS-5 distributions of the P-wave velocity changes show good coincidence with the pre-existing macroscopic structure as shown in the right photo.

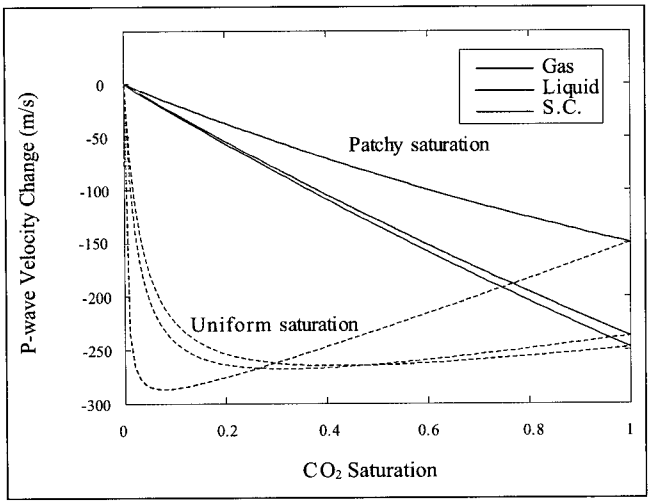

Fig. 9. Theoretical estimation of P-wave velocity reduction due to presence of CO_2 for two extreme cases: uniform saturation and patch saturation. See text for details.

other paths during injection of CO_2, for all three cases. This result suggests that the injected CO_2 migrated through an area that has a limited number of narrow channels, as indicated by a slightly deeper red colour in the P-wave velocity images in Figures 6a, 7a, and 8a. If the pores around this path are much finer ones, CO_2 will have difficulty in penetrating such narrow-pore zones, especially because capillary forces may prevent penetration. In other words, displacement will be inefficient in finer pore spaces because of capillary effects caused by the relatively high interfacial tension between CO_2 and water. Water is usually more wetting than CO_2, and CO_2 displacement will prefer larger pore spaces. This process usually causes greater velocity reduction in unconsolidated sandstones than in consolidated sandstones (Wang and Nur, 1989; Xue et al., 2005). Capillary pressure amplifies the effects of heterogeneity, with CO_2 bypassing larger volumes of water. This fingering behaviour allows only a small fraction of the pore volume of the reservoir to be available for sequestration, resulting in an increase in the cost of CO_2 sequestration in saline aquifers.

Applications of seismic tomography in CO_2 monitoring

For CO_2 monitoring, we are more interested in the relative change of seismic velocity caused by CO_2 injection than the absolute velocity distribution. The effect of CO_2 injection on the velocities measured in the laboratory has been examined for different phases of CO_2. By directly using differential arrival times, determined manually by comparison of two consecutive waveforms along the same path, the difference tomography method is able to image the velocity change during injection of CO_2. Temporal-spatial distributions of relative velocity change were well imaged. Such distributions of velocity change reflect CO_2 (either gaseous, liquid, or supercritical) migration in the water-saturated samples.

The ability to use the cross-hole seismic tomography method to monitor CO_2 depends strongly on the velocity changes caused by CO_2 injection. Seismic tomographic results obtained from injection of supercritical CO_2 showed the highest velocity decrease among the three injection cases. Therefore, seismic methods, especially high-frequency, high-resolution seismic methods, are expected to be useful in monitoring CO_2 flooding processes or in detecting CO_2 zones in the subsurface. In field experiments, observed velocity changes due to the presence of CO_2 have been confirmed at seismic and sonic frequencies (Saito et al., 2005; Xue et al., 2005). When the frequency of the applied seismic wave is high enough that the wavelength is less than the size of inhomogeneities, the patchy saturation model can be used and the seismic velocity decreases almost linearly with CO_2 fraction. In such conditions, CO_2 fraction can be estimated from velocity data. Here we will meet another difficulty if the size of inhomogeneous patches is also unknown. As a suggestion, a valuable approach may be to investigate seismic responses at multiple frequencies over as wide a range as possible.

ACKNOWLEDGMENTS

We thank Osamu Nishizawa of AIST for his thoughtful review comments, which have helped substantially to improve this paper. Thanks also to an anonymous reviewer for his constructive comments. This work was supported by the Ministry of Economy, Trade, and Industry of Japan under the contract: "Research and Development of Underground Storage Technology for Carbon Dioxide".

REFERENCES

Arts, R., Eiken, O., Chadwick, A., Zweigel, P., van der Meer, L., and Zinszner, B., 2004, Monitoring of CO_2 injected at Sleipner using time lapse seismic data: *Energy*, **29**, 1383–1392.

Benson, S.M., 2005, Overview of geological storage of CO_2: in Thomas, D., and Benson, S.M. (eds), *Carbon Dioxide Capture for Storage in Deep Geologic Formations*, Volume 2, Elsevier Science, 665–672.

Chadwick, R.A., Eiken, O., and Lindeberg, E., 2004, 4D geophysical monitoring of the CO_2 plume at Sleipner, North Sea: Aspects of uncertainty: *Proceedings of the 7th SEGJ International Symposium, Sendai*, November, 24–26.

Gassmann F., 1951, Über die Elastizität poröser Medien: *Vierteljahrsschrift der Naturforschenden Gesellschaft in Zürich*, **96**, 1–23.

Garćia, J., and Pruess, K., 2003, Flow instabilities during injection of CO_2 into saline aquifers: *Proceedings of TOUGH Symposium, Lawrence Berkeley National Laboratory, Berkeley, California*, May, 12–14.

Harris, J.M., Nolen-Hoeksema, R.C., Van Schaack, M., Lazaratos, S.K., and Rector, J.W., 1995, High-resolution crosswell imaging of a west Texas carbonate reservoir: Part I - Project summary and interpretation: *Geophysics*, **60**, 667–681.

Hoversten, G.M., and Myer, L.R., 2000, Monitoring of CO_2 sequestration using integrated geophysical and reservoir data: in Williams, D., Durie, B., McMullan, P., Paulson, C., and Smith, A. (eds), *Proceedings of the 5th International Conference on Greenhouse Gas Control Technologies (GHGT5)*, 305–310.

Li, G., 2003, 4D seismic monitoring of CO_2 flood in thin fractured carbonate reservoir: *The Leading Edge*, **22**, 690–695.

Mavko, G., and Mukerji, T., 1998, Bounds on low-frequency seismic velocities in partially saturated rocks: *Geophysics*, **63**, 3, 918–924.

Saito, H., Azuma, H., Nobuoka, D., Tanase, D. and Xue, Z., 2005, Time-lapse crosswell seismic tomography monitoring of CO_2 at an onshore aquifer, Nagaoka, Japan: *Exploration Geoophysics*, **37**, (this issue).

Van der Meer, L., 1992, Investigations regarding the storage of carbon dioxide in aquifers in the Netherlands: *Energy Conversion and Management*, **33**, 611–618.

Wang, Z., and Nur, A., 1989, Effects of CO_2 flooding on wave velocities in rocks with hydrocarbons: *Society of Peteroleum Engineers, Reservoir Engineering*, **3**, 429–439.

Wang, Z., Cates, M., and Langan, R., 1998, Seismic monitoring of a CO_2 flooding in a carbonate reservoir: A rock physics study: *Geophysics*, **63**, 1604–1617.

Xue, Z., Ohsumi, T., 2004a, Seismic wave monitoring of CO_2 migration in water-saturated porous sandstone: *Butsuri-Tansa*, **57**, 25–32.

Xue, Z., Ohsumi, T., 2004b, Laboratory measurements on gas permeability and P-wave velocity in two porous sandstones during CO_2 flooding: *Journal of the Mining and Materials Processing Institute of Japan*. **120**, 91–98.

Xue, Z., Ohsumi, T., 2005, Experimental studies on seismic monitoring of CO_2 in geological sequestration: *Journal of the Japanese Association of Groundwater Hydrology*, **47**, 29–44.

Xue, Z., Tanase, D., and Watanabe, J., 2005, Estimation of CO_2 saturation from time-lapse well logging in an onshore aquifer, Nagaoka, Japan: *Exploration Geoophysics*, **37**, (this issue).

弾性波トモグラフィによる多孔質砂岩中のCO_2挙動モニタリングの実験的研究

薛　自求[1]・雷　興林[2]

要　旨：　含水飽和状態の砂岩試料に気体，液体及び超臨界 CO_2 をそれぞれ注入し，CO_2 と間隙水との置換による P 波速度の変化を測定した。これらの測定実験には多胡砂岩を用いており，CO_2 注入によって P 波速度は平均で約６％減少し，超臨界 CO_2 の注入実験では最大で約１６％と大きく減少した。さらに，いずれの注入ケースにおいても円柱試料の長軸方向が堆積層理面と平行する試料の方が直交するものよりも P 波速度の減少率が大きかった。このような堆積層理面の影響は P 波速度の変化に基づくトモグラフィ解析結果でも認められた。注入された CO_2 の浸透挙動については，長軸方向が堆積層理面と直交する試料の方がより複雑であったことが明らかになった。また，トモグラフィのイメージでは注入された CO_2 の状態や孔隙の不均質性による違いも確認することができた。これらの実験結果は地中貯留における CO_2 挙動モニタリング手法として，弾性波トモグラフィの有効性が示されたと考えられる。

キーワード：速度差トモグラフィ、P 波速度、多孔質砂岩、CO_2 モニタリング、堆積層理面、異方性

P-파 속도 영상화에 근거한 물로 포화된 이방성 사암에서의 CO_2 이동에 관한 실험 연구

Ziqiu Xue[1] and Xinglin Lei[2]

요　약：　물로 포화된 이방성 사암에 기체상, 액체상, 그리고 초임계상의 CO_2 를 주입하면서 P 파의 속도 변화를 측정하였다. 층리면에 수직한 방향과 수평 방향을 따라 시추한 2 개의 원통 모양의 Tako 사암들에 압전 송수신 배열 시스템을 이용하여 P 파 속도를 측정하였다. CO_2 주입으로 인한 속도 변화는 일반적으로 -6%의 평균값을 보였으며 초임계상의 CO_2 를 주입하는 경우에 약 -16%의 최대값을 나타냈다. 차분도착주시법(differential arrival-time)으로부터 얻은 P 파 속도 토모그램은 CO_2 의 유동이 층리면에 평행할 때보다 수직한 경우 CO_2 의 이동 양상이 더 복잡하다는 것을 명백히 보여주고 있다. 또한 P 파 속도 영상의 차이가 CO_2 의 상과 암석내 공극분포의 불균질성과 관련되었음을 발견하였다. 초임계상의 CO_2 를 주입한 경우, 탄성파 영상은 기체상과 액체상의 CO_2 를 주입한 경우에 비해 가장 큰 속도 감소를 보였다. 이 결과는 지중 격리시 CO_2 모니터링에 대한 탄성파 방법의 효용을 확신시켜 줄 것이다.

주요어：차이 토모그라피, P 파 속도, 다공성 사암, CO_2 모니터링, 층리면, 이방성

1 地球環境産業技術研究機構
〒619－0292　京都府相楽郡木津町木津川台 9-2
2 産業技術総合研究所　地質情報研究部門

1 Research Institute of Innovative Technology for the Earth

2 산업기술종합연구소 지질정보연구부문